energies

MDPI

Article

Numerical Study of the Effects of Thermal Barrier Coating and Turbulence Intensity on Cooling Performances of a Nozzle Guide Vane

Prasert Prapamonthon *, Huazhao Xu, Wenshuo Yang and Jianhua Wang *

Department of Thermal Science & Energy Engineering, School of Engineering Science, University of Science and Technology of China, Hefei 230027, China; xuhz@ustc.edu.cn (H.X.); wenshuo@mail.ustc.edu.cn (W.Y.)

* Correspondences: jinfa@mail.ustc.edu.cn (P.P.); jhwang@ustc.edu.cn (J.W.); Tel.: +86-551-6360-0945 (P.P. & J.W.)

Academic Editor: Michael Walls
Received: 6 January 2017; Accepted: 9 March 2017; Published: 14 March 2017

Abstract: This work presents a numerical investigation of the combined effects of thermal barrier coating (TBC) with mainstream turbulence intensity (*Tu*) on a modified vane of the real film-cooled nozzle guide vane (NGV) reported by Timko (NASA CR-168289). Using a 3D conjugate heat transfer (CHT) analysis, the NGVs with and without TBC are simulated at three *Tus* (*Tu* = 3.3%, 10% and 20%). The overall cooling effectiveness, TBC effectiveness and heat transfer coefficient are analyzed and discussed. The results indicate the following three interesting phenomena: (1) TBC on the pressure side (PS) is more effective than that on the suction side (SS) due to a fewer number of film holes on the SS; (2) for all three *Tus*, the variation trends of the overall cooling effectiveness are similar, and TBC plays the positive and negative roles in heat flux at the same time, and significantly increases the overall cooling effectiveness in regions cooled ineffectively by cooling air; (3) when *Tu* increases, the TBC effect is more significant, for example, at the highest *Tu* (*Tu* = 20%) the overall cooling effectiveness can increase as much as 24% in the film cooling ineffective regions, but near the trailing edge (TE) and the exits and downstream of film holes on the SS, this phenomenon is slight.

Keywords: thermal barrier coating; overall cooling effectiveness; nozzle guide vane

1. Introduction

It is well-known that internal convection and impingement cooling, film cooling, and thermal barrier coatings (TBCs) are major techniques, which are widely used to protect gas-turbine airfoils from high turbine inlet temperatures (TITs) and achieve the maximum thermal efficiency in state-of-the-art gas turbine engines. In fact, the film cooling is an effective method related to the internal cooling, and film cooling performances are influenced by many factors, such as the configuration and position of the film hole, adverse pressure gradient, boundary layer thickness, mainstream turbulence intensity (*Tu*) and length scale (*Lu*), and the amount of cooling air consumption. Boyle et al. [1] deemed that *Tu* and *Lu* were two physical factors, which naturally and significantly affected the film cooling performances amid those factors. Mayhew et al. [2] expected that real gas-turbine engines were frequently operated under *Tu* at about 10%–20%. The effects of *Tu* on the film cooling performance and heat transfer coefficient of turbine airfoils, cylindrical leading edge and flat plate models have been experimentally and numerically investigated by previous researches [3–8]. To prolong and give good service to the turbine airfoils, TBC has been widely utilized in gas turbine designs as a thermal insulator between hot mainstream and metal surfaces. The insulating thermal capabilities of TBC are affected by many factors, such as porosity, thickness, thermal conductivity, and phase stability of the TBC material as well as the TIT and *Tu* of hot gas as reported by researches [9–14].

Recently, CHT analysis has been commonly applied to predict the real metal surface temperatures and cooling performances of turbine vanes. In the numerical investigations of previous works [15–18], CHT analysis was used to study the film cooled vanes without TBC. Using a Mark II vane provided by Hylton et al. [19], Bohn and Becker [20] used 3D CHT analysis and a Baldwin-Lomax turbulence model [21] to study the aerodynamic and thermal effects of the vane without and with TBC (ZrO_2, 0.3 mm thickness). Their work indicated that TBC reduced metal temperatures by about 20–29 K in the stagnation area and about 27–43 K in shock area on the suction side (SS). However, TBC hardly affected the metal temperatures near the trailing edge (TE). With the same method and vane model, Bohn and Tümmers [22] investigated the effects of TBC and cooling air flow rate on the thermal stresses within the vane structure, their work concluded that the influence of the thermal resistance added by TBC on the thermal stresses was significantly higher than the influence due to reducing the cooling air flow rate. Alizadeh et al. [23] used CHT analysis and a shear stress transport (SST) k-ω turbulence model to investigate the effects of the thickness and thermal conductivity of TBC on the cooling performances of a turbine blade. Their research indicated that adding a 0.2 mm TBC could result in a 19 K and 34 K fall in the average and maximum temperatures, respectively. But, if the thermal conductivity of TBC increased from 1 W/m·K to 3 W/m·K, the average temperature rose about 10 K. Rossette et al. [24] used CHT analysis and a Spalart-Allmaras turbulence model [25] to investigate the aero-thermal performance of a first stage gas turbine blade with TBC. They concluded that an increase in TBC thickness by about 100–400 µm could reduce the surface temperature by up to 200 K, and TBC could reduce cooling air consumption by about 36% cooling air consumption to maintain the creep life of the blade materials. However, the above literatures focused on the models of the airfoils with a TBC effect only, and no film holes were included.

Nowadays, in advanced gas turbine vane designs, TBC and film cooling are synchronously used, and the real gas-turbine vanes or blades operate in the *Tu* range of 10%–20%. Therefore, it is necessary to provide the designers and investigators of gas-turbine vanes with relatively comprehensive information related to the combined effects of TBC and *Tu* on the real cooling performances using a 3D CHT analysis.

2. Thermal Parameters

Figure 1 illustrates the definitions of thermal parameters in Equations (1)–(6). Since the thickness of the TBC layer is thin, therefore a 1D heat conduction effect within the layer is assumed. This means that heat transfers only in the direction normal to the surface.

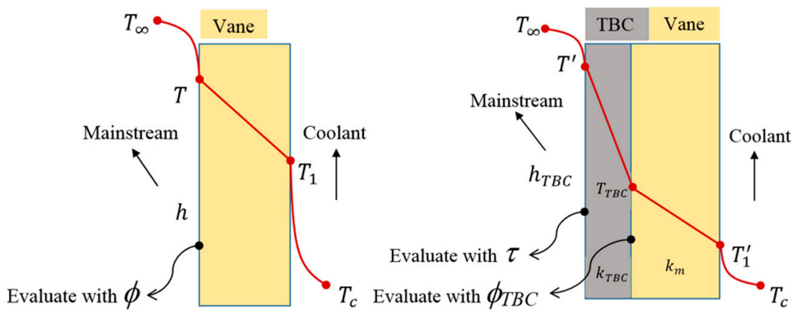

Figure 1. Evaluation thermal parameters on vane surface with and without thermal barrier coating.

(1) Overall cooling effectiveness (ϕ):

$$\phi = \frac{T_\infty - T_w}{T_\infty - T_c} \tag{1}$$

where $T_w = \begin{cases} T\text{ , uncoated vane } \Rightarrow \phi \\ T_{TBC}\text{ , coated vane } \Rightarrow \phi_{TBC} \end{cases}$. This parameter is used to evaluate the cooling performance on the outside metal surface using the CHT analysis.

(2) TBC effectiveness (τ):

$$\tau = \frac{T_\infty - T'}{T_\infty - T_c} \tag{2}$$

This parameter is defined to discuss the effect of TBC on the outside temperature of TBC.

(3) Percentage of temperature reduction (R):

$$R = \left(1 - \frac{T_{TBC}}{T}\right) \times 100\% \tag{3}$$

This parameter is used to evaluate the ability of TBC to reduce the metal temperature of the vane.

(4) Increment of overall cooling effectiveness ($\Delta\phi$):

$$\Delta\phi = \left(\frac{\phi_{BC} - \phi}{\phi}\right) \times 100\% \tag{4}$$

This parameter is used to evaluate the effect of TBC on the metal temperature at each Tu.

(5) Variation of heat transfer coefficient (Δh):

$$\Delta h = h - h_{TBC} \tag{5}$$

$$\text{where } h = \frac{q_{flux}}{T_\infty - T_w} = \frac{-k_f\left(\frac{\partial T}{\partial n}\right)_{w=0}}{T_\infty - T_w} \tag{6}$$

It is worth noting that the heat transfer coefficient defined by Equation (6) is based on the local wall surface temperature and mainstream temperature. A negative h means that heat transfers from the surface to the mainstream. On the other hand, h is positive when heat transfers from the mainstream to the vane surface.

3. Geometric Configuration

The geometry referenced in this work is a modified vane of the film-cooled nozzle guide vane (NGV) reported by Timko [26], which consists of enhanced internal cooling with a forward and an aft cavity, and external film cooling with a total of 13 rows with 199 holes, as shown in Figure 2a,b. The height of NGV is 4 cm, and a constant cross-section view at midspan is given in Figure 2c. Two rows of diffusion shaped-holes, $R1$ and $R2$, are placed on the SS. Rows $R3$ to $R9$ of the film holes are cylindrical with the same size and angle in the radial direction, and all of them are located at the leading edge (LE) and its vicinity. Two rows of the compound angled type, $R10$ and $R11$, and one row of the film holes in the axial direction, $R12$, are drilled on the pressure side (PS), and one row of slot, $R13$, is positioned at the TE. More details about the film holes are presented in Table 1.

Table 1. Details of film holes [26].

Row	Number of Holes	Hole Diameter (cm)	Type/Angle
1	22	0.061	Axial, Diffusion shaped
2	23	0.061	Axial, Diffusion shaped
3	12	0.048	Radial
4	12	0.048	Radial
5	12	0.048	Radial
6	12	0.048	Radial
7	12	0.048	Radial
8	12	0.048	Radial
9	12	0.048	Radial
10	20	0.036	Compound Angle 45°
11	16	0.061	Compound Angle 60°
12	16	0.048	Axial
13	18	0.061 × 0.155	Pressure side slot

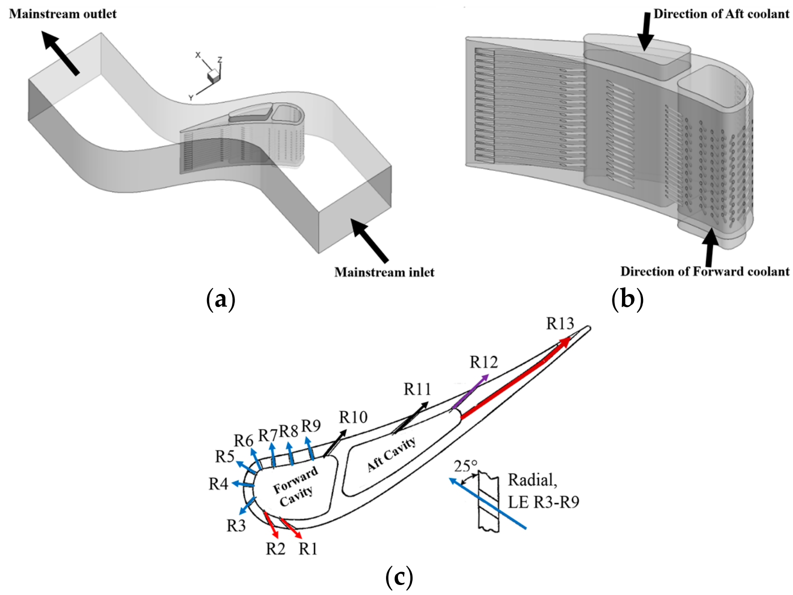

Figure 2. (**a**) Mainstream cascade; (**b**) Vane configuration; (**c**) Cross-section area of the vane at midspan.

4. Computational Procedures

4.1. Computational Mesh

All numerical meshes are of a hexahedral unstructured type, which are generated by ANSYS ICEM V.15 using the tools of blocking manipulation. To obtain high qualities, the meshes are further adapted by R and H refinement procedures. In addition, the O-grid scheme is applied to the fluid region in the immediate vicinity of the vane walls to resolve the boundary layer flows. Three numbers of elements with coarse mesh 9,143,910 (9.1 M), medium mesh 10,672,683 (10.6 M), and fine mesh 13,171,055 (13 M) are compared to assure that the numerical results are independent of the mesh strategy. Figure 3a,b shows the dimensionless pressure and surface temperature distributions along the vane surface at midspan, respectively. The medium and fine mesh strategies give acceptable agreements to each other. The maximum difference for the temperature is less than 2%. Therefore, it is reasonable to choose the medium mesh with 10.6 M elements for the following calculations. The value of y^+ in the current simulation is less than 5, which is generally acceptable. Detailed reviews of some computational meshes and the quality distribution of the computational mesh are depicted in Figure 4a,b, respectively.

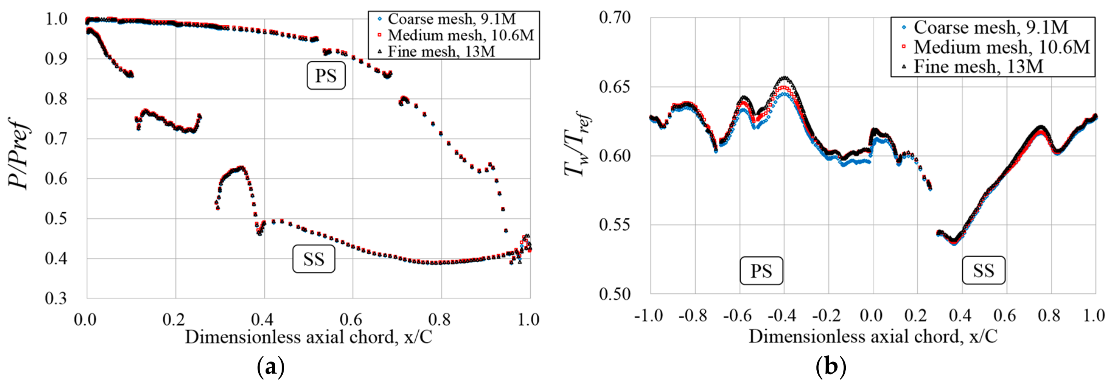

Figure 3. (**a**) Pressure; (**b**) temperature distributions of three meshes at midspan.

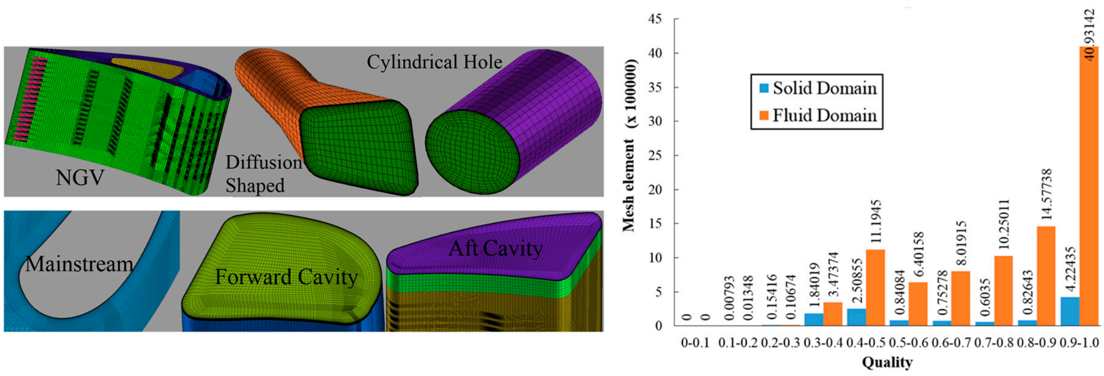

Figure 4. (**a**) Computational mesh; (**b**) quality distribution of computational mesh.

4.2. Calculation Techniques

ANSYS FLUENT V.15 is used as the solver, and the SST k-ω turbulence model with a Semi-Implicit Method for Pressure-Linked Equations (SIMPLE) algorithm is implemented appropriately. The spatial discretization with second order accuracy is used to solve momentum and energy equations in the fluid domains, whereas in the solid domain only the energy equation is solved on the basis of Fourier's law. Under-relaxation factors are adjusted attentively to obtain the converged results. The convergence criteria of the results are that the residual magnitudes of energy and continuity equations must reduce to the levels of 10^{-6} and 10^{-3}, respectively. Moreover, the converged results are substantiated by proving the balance of mass flow rates at all inlets and outlets, and observing the traces of temperature variation at monitoring points on the vane surfaces. The Mesh Interface Technique (MIT) is applied to deal with all couple interfaces of solid-fluid domains. In order to numerically study the effects of TBC, all elements at the interfaces of the vane and fluid mainstream are applied to a layer of TBC with a uniform thickness of 0.3556 mm, as reported by Halila et al. [27]. For this thin layer of TBC, only 1D heat conduction equation is solved.

The fluid domain consists of cooling air and a hot mainstream, the vane is made of steel, and TBC is ZrO_2, and the thermal properties are given in Table 2.

Table 2. Properties of air, steel [28,29] and TBC.

Property of Material	Air: Mainstream and Cooling Air	Steel: Vane Structure	ZrO_2: TBC
Density (kg·m^{-3})	ρ_f = ideal gas assumption	$\rho_m = 8055$	$\rho_{TBC} = 5500$
Specific heat capacity (J·kg^{-1}·K^{-1})	$c_{p,f} = 938 + 0.196$ T	$c_{p,m} = 438.5 + 0.177$ T	$c_{p,TBC} = 418$
Thermal conductivity (W·m^{-1}·K^{-1})	$k_f = 0.0102 + 5.8 \times 10^{-5}$ T	$k_m = 11.2 + 0.0144$ T	$k_{TBC} = 1.04$
Viscosity (kg·m^{-1}·s^{-1})	Three-equation of Sutherland model	-	-

4.3. Boundary Conditions

Numerical simulations are carried out under the boundary conditions reported by Timko [26], as shown in Table 3. It should be noted that five exact pressure ratios (*PRs*), i.e., *PR* = 1.67, 2.0, 2.3, 2.5, and 2.7 were used in Timko's report [26], but it lacks the specification of the exact *PR* used to obtain the experimental results. Therefore, it is worth testing simulations at those *PRs*. To save the computational cost and time, *PR* = 1.67, 2.3 and 2.7 are tested, and the designed *PR* of 1.67 is used for all simulations. Three *Tus* (*Tu* = 3.3%, 10% and 20%) at the mainstream inlet are added to study the *Tu* effects on the cooling performances in the following section. Due to the lack of exact values from Timko [26], the length scale, *Lu*, is set at a constant value of 6 cm at the inlet of the mainstream following the instruction of FLUENT V.15.

Table 3. Basic boundary conditions used in all simulations.

Boundary	Condition
Mainstream inlet	T_∞ = 709 K, $P_{T,\infty}$ = 3.44740 × 10^5 Pa, Lu = 6 cm, Tu = 3.3%, 10% and 20%
Mainstream outlet	PR = 1.67, Intended PR of Timko [26]
Forward coolant inlet	T_c = 339 K, $P_{T,c}$ = 3.50950 × 10^5 Pa
Forward coolant outlet	Adiabatic wall with non-slip condition
Aft coolant inlet	T_c = 339 K, $P_{T,c}$ = 3.50950 × 10^5 Pa
Aft coolant outlet	Adiabatic wall with non-slip condition

4.4. Validation of the Turbulence Model

All of the numerical results in this work are carried out using a SST k-ω turbulence model, which has been tested successfully in predicting flow and thermal fields by several researchers [17,18,23,30]. To validate the results obtained from the SST k-ω turbulence model, the numerical Mach number (Ma) along the vane surface at midspan is compared against the experimental data reported by Timko [26] at PR = 1.67, 2.3, and 2.7, as shown in Figure 5. For the three PRs, in the regions of $0 < x/C < 0.4$ on the SS and $0 < x/C < 0.5$ on the PS, the numerical results of Ma give acceptable agreements with the experimental data, and the effect of PR on Ma is insignificant. But, at PR = 1.67, the numerical result of Ma is underestimated at $x/C \approx 0.61$ and 0.68 on the PS. With PR increasing up to 2.3 and 2.7, the numerical results of Ma at those positions rise up close to the experimental data with a maximum error of about 10%. This indicates that the differences between the numerical results and the experimental results of Ma meaningfully decrease with PR, and the SST k-ω turbulence model can provide acceptable results in this work. However, it should be noted that PR = 1.67 is used for all simulations in this work because it was the design condition reported by Timko [26].

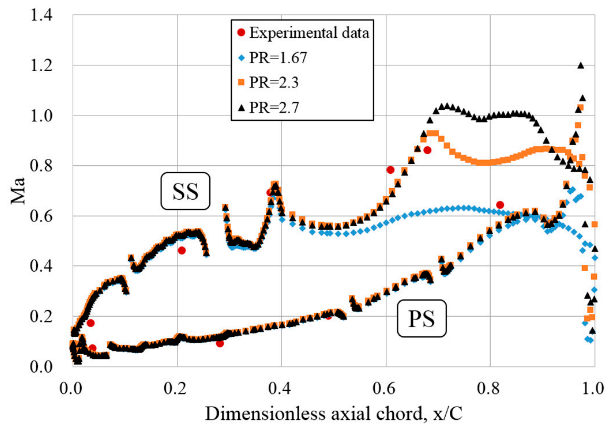

Figure 5. Mach number distributions along vane surface at midspan.

5. Results and Discussions

5.1. Overall Cooling Effectiveness and TBC Effectiveness

Figure 6a compares the ϕ_{TBC} and ϕ distributions at midspan for the three Tus. It is observed that at the same Tu, ϕ_{TBC} is always higher than ϕ, because T_{TBC} is always lower than T. However, the distributions of ϕ and ϕ_{TBC} are similar to each other. The higher ϕ and ϕ_{TBC} are at the exits of the film holes, and the highest ϕ and ϕ_{TBC} are found at the same position, i.e., x/C = 0.38 on the SS. It means that this position has the lowest T and T_{TBC}. The reason is that the position is just downstream of shaped-holes $R1$ and $R2$, where the combined effects of the larger number of film holes and the lower pressure on the SS, including reduced effective blowing ratio at the hole exits [31] can effect more cooling air to be emitted from the film holes. When Tu increases, ϕ and ϕ_{TBC} decrease, because

T and T_{TBC} increase with Tu. But, these effects on ϕ and ϕ_{TBC} are relatively smaller in the region of $0.4 < x/C < 0.7$ on the SS, the reason is that the effect of Tu on the SS is much less sensitive than that on the PS. Figure 6b illustrates the noteworthy differences between τ and ϕ_{TBC} at midspan for the three *Tus*. At the same Tu, τ is lower than ϕ_{TBC} except at the exits of the film holes, where τ may be equal to or higher than ϕ_{TBC}. Moreover, τ is close to ϕ_{TBC} in the region of $0.38 < x/C < 0.6$ on the SS, and the distributions of τ are consistent with T'. These phenomena suggest that the TBC does not play a major role near the exits of the film holes and the effectively cooled regions. Like ϕ and ϕ_{TBC}, an increase in Tu only causes a quantitative reduction in τ, and the trends of the τ distributions retain the same.

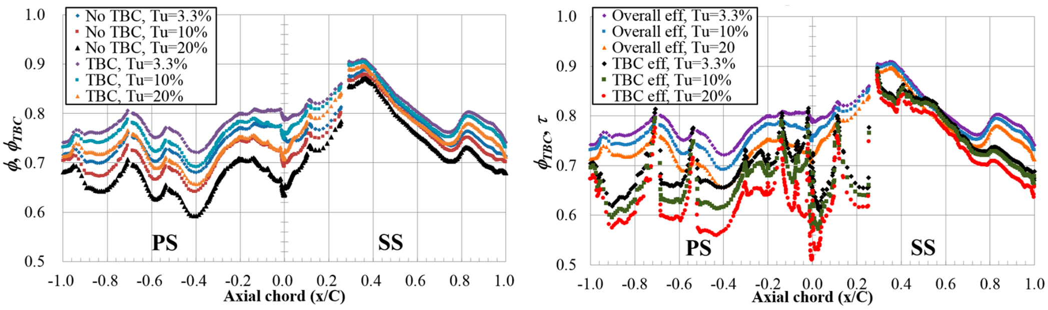

(**a**) (**b**)

Figure 6. Comparisons between (**a**) overall cooling effectiveness without (ϕ) and with (ϕ_{TBC}) thermal barrier coating; (**b**) ϕ_{TBC} and TBC effectiveness (τ) at midspan and turbulence intensity (Tu) = 3.3%, 10% and 20%.

Figures 7 and 8 present the holistic contours of ϕ, ϕ_{TBC}, and τ on the PS and the SS, for the three *Tus*, respectively. From those figures, the following interesting phenomena can be observed: (1) at the same Tu, τ is of the lowest effectiveness in general except at the exits of the film holes, and ϕ_{TBC} is always higher than ϕ. Moreover, the distributions of ϕ and ϕ_{TBC} are more uniform than that of τ due to the lower thermal conductivity of TBC. The distribution of τ is similar to the distributions of the adiabatic film effectiveness obtained by adiabatic assumption in our previous work [28,29]. This phenomenon is reasonable because the thermal conductivity of TBC is much lower than that of the vane's material, and TBC reduces the heat flux transferred into the solid structure; (2) At each Tu, the relatively lower τ, ϕ, and ϕ_{TBC} always happen near the tip and the hub of the vane, because it is difficult to cool those regions effectively by the cooling air emitted from the film holes. However, the relatively higher τ, ϕ, and ϕ_{TBC} always happen at the exits and downstream of the diffusion shaped-holes $R1$ and $R2$ on the SS; (3) When Tu increases, the regions with the relatively lower effectiveness at the tip and hub expand significantly, which is as expected since more heat is transferred to the vane with higher *Tus*.

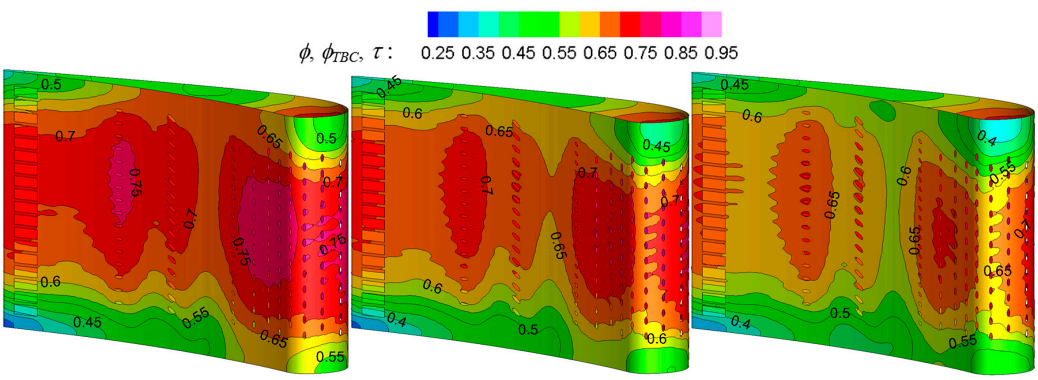

ϕ: (**a**) Tu = 3.3% (**b**) Tu = 10% (**c**) Tu = 20%

Figure 7. *Cont.*

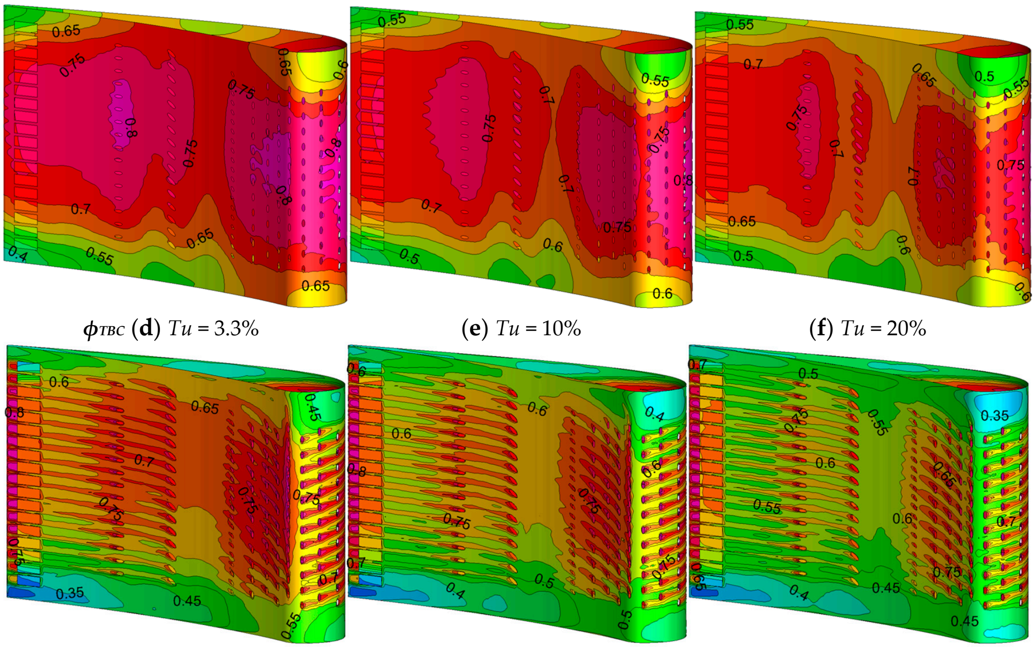

ϕ_{TBC} (**d**) *Tu* = 3.3% (**e**) *Tu* = 10% (**f**) *Tu* = 20%

τ (**g**) *Tu* = 3.3% (**h**) *Tu* = 10% (**i**) *Tu* = 20%

Figure 7. Contours of (**a**–**c**) ϕ; (**d**–**f**) ϕ_{TBC}; (**g**–**i**) τ on the pressure side (PS) at three *Tus*.

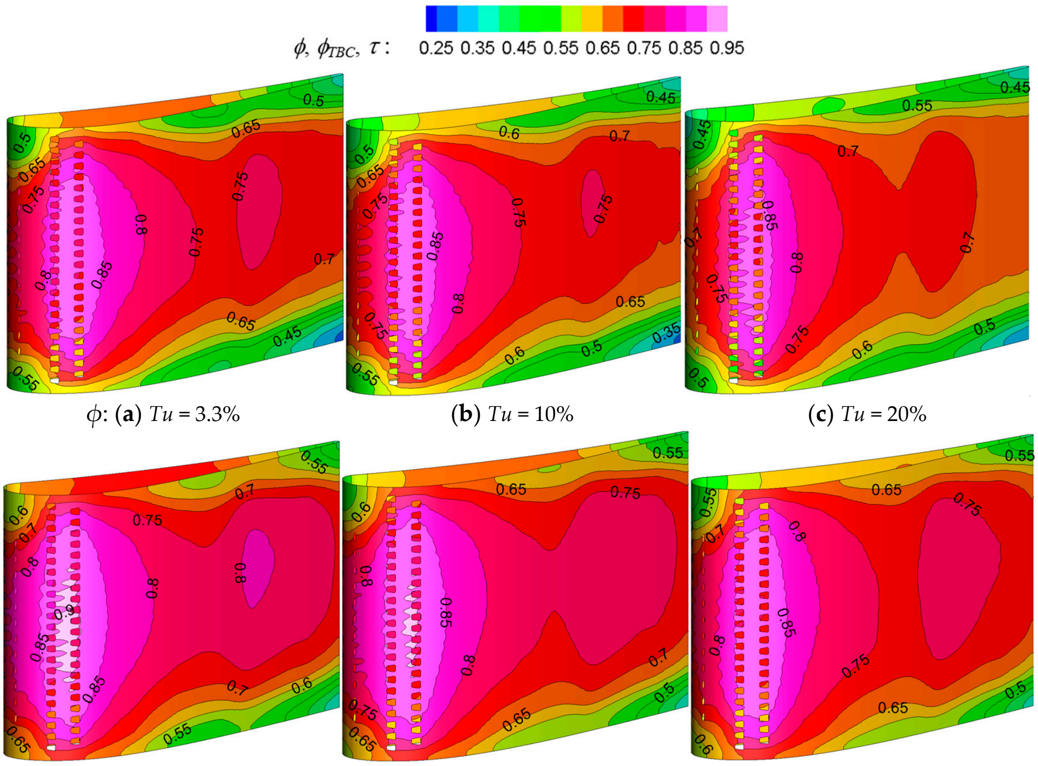

ϕ: (**a**) *Tu* = 3.3% (**b**) *Tu* = 10% (**c**) *Tu* = 20%

ϕ_{TBC} (**d**) *Tu* = 3.3% (**e**) *Tu* = 10% (**f**) *Tu* = 20%

Figure 8. *Cont*.

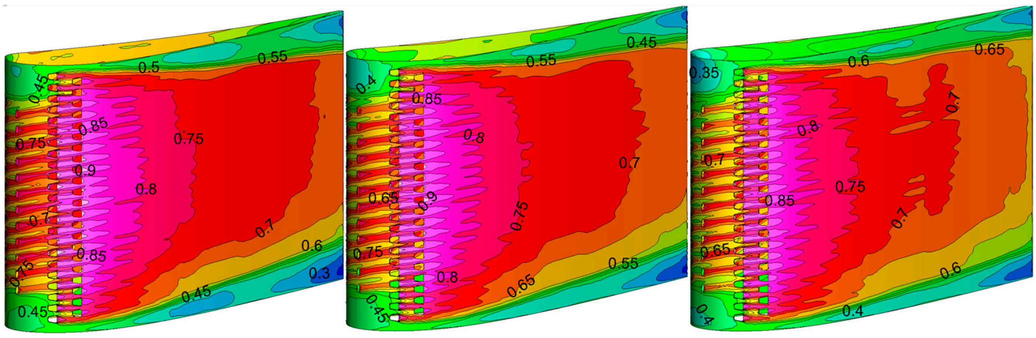

τ (**g**) *Tu* = 3.3% (**h**) *Tu* = 10% (**i**) *Tu* = 20%

Figure 8. Contours of (**a–c**) ϕ; (**d–f**) ϕ_{TBC}; (**g–i**) τ on the suction side (SS) at three *Tus*.

Additionally, the ability of TBC is quantitatively evaluated by the percentage of temperature reduction, R, defined in Equation (3), for the three *Tus*, as shown at midspan in Figure 9. It is obvious that for each *Tu*, the value of R increases in the region of $0.6 < x/C < 0.9$ on the SS and $-0.8 < x/C < -0.2$ on the PS, but rapidly drops near the TE, i.e., $-1.0 < x/C < -0.9$ and $0.95 < x/C < 1.0$. The highest values for R (R = 5% at Tu = 3.3% and R = 6% at Tu = 20%) are at the same position, i.e., $x/C = -0.8$, which is between the film rows $R12$ and $R13$ on the PS. The lowest R is about 1.1% at Tu = 3.3% and 1.7% at Tu = 20% in the region from x/C = 0.38 to x/C = 0.6 on the SS, where T', T, and T_{TBC} are at the lowest values, because those are the positions of the exits and are downstream of the shaped-holes in $R1$. Moreover, the results also indicate that the value of R on the PS is generally higher than that on the SS. This result is different from the conclusion drawn by Meitner [13], which concluded that TBC was more effective on the *SS* than on the PS because the heat flux was higher on the uncoated SS. Nevertheless, the conclusion in this work is still reasonable because the amount of film-hole rows on the SS is much less than that in Meitner [13]. Therefore, the heat flux is higher on the uncoated PS, as shown in Figure 10. These phenomena indicate that the role of TBC on the PS is more dominant than that on the SS due to a fewer number of film holes, and this role decreases in the regions cooled effectively by the cooling air discharged from the film holes as well as the TE. With increasing in *Tu*, it is found that the increases of R in the effectively cooled regions near $R1$ and the TE are smaller than those in other regions.

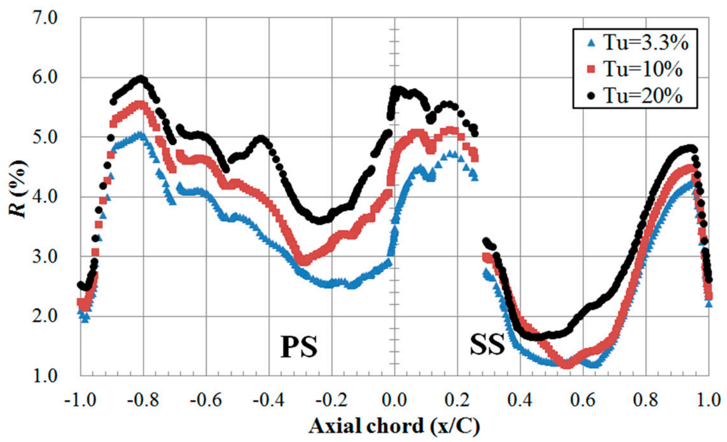

Figure 9. Effect of *Tu* on the percentage of temperature reduction (R) at midspan.

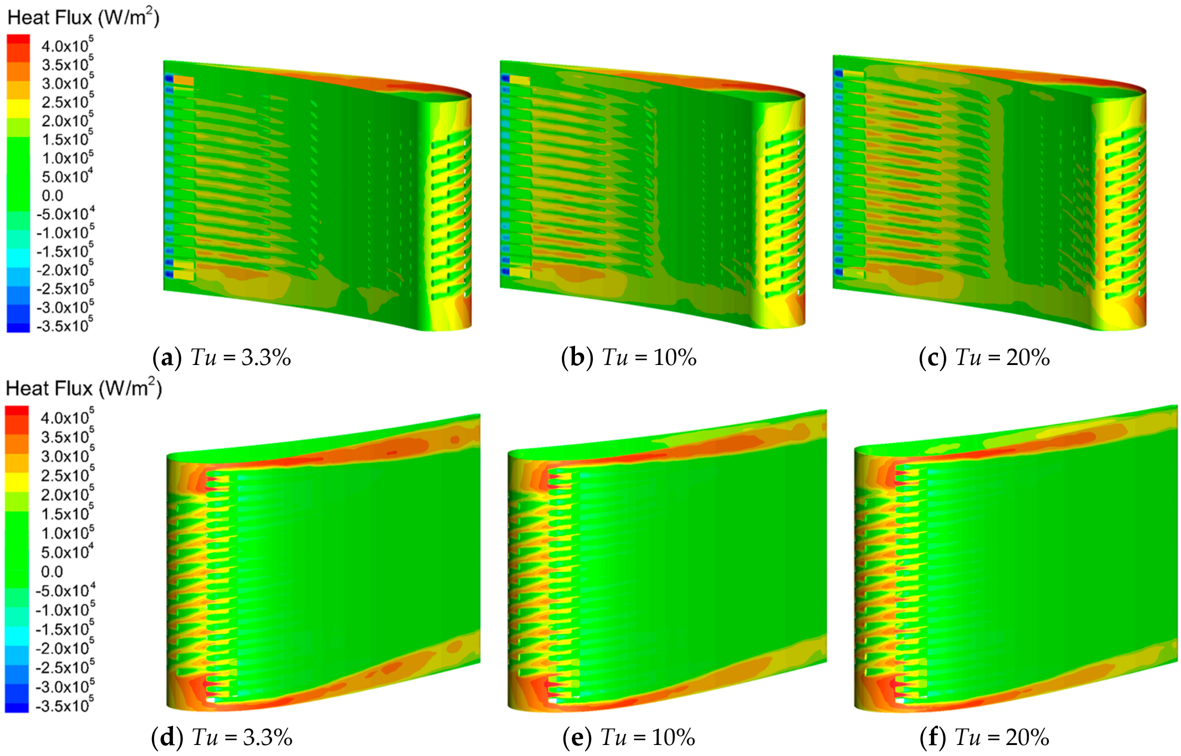

Figure 10. Heat flux on the uncoated vane (**a**–**c**) on the PS; (**d**–**f**) on the SS at three *Tus*.

5.2. Effects of TBC and Tu on Overall Cooling Effectiveness

Figure 11 presents the effects of TBC on increasing in the overall cooling effectiveness in percentage on the vane surfaces for the three *Tus*. One can find three important phenomena: (1) at each *Tu*, the values of $\Delta\phi$ are always positive. This means that TBC plays a constructive role to protect the vane, especially at the tip and the hub as marked as A to F, which are the locations cooled poorly by cooling air; (2) at each *Tu*, this constructive role is weaker at the exits and downstream of the diffusion shaped-holes *R*1 on the SS, and the regions near the TE as marked as *X* and *Y*; (3) With increasing in *Tu*, the constructive role is more significant, namely at higher *Tus*, the overall cooling effectiveness demonstrates a significant improvement by TBC in the regions near the tip (Region A, $\Delta\phi$ = 18%, 24% and 24% or ΔT = 32 K, 38 K and 38 K for *Tu* = 3.3%,10% and 20%, respectively) and near the hub (Region C, $\Delta\phi$ = 16%, 19% and 21% or ΔT = 34 K, 36 K and 38 K for *Tu* = 3.3%, 10% and 20%, respectively) on the LE-SS. But, the improvement becomes slight in the regions of downstream of the diffusion shaped-hole *R*1 on the SS ($\Delta\phi$ = 2%, 2%–3% and 3% or ΔT = 6 K, 6–8 K and 8 K for *Tu* = 3.3%, 10% and 20%, respectively) and near the TE. These results exhibit the benefits of introducing TBC to protect NGV from harsh mainstream flows, especially for the regions which are insufficiently cooled by cooling air, and TBC effects an increase in the overall cooling effectiveness when *Tu* increases.

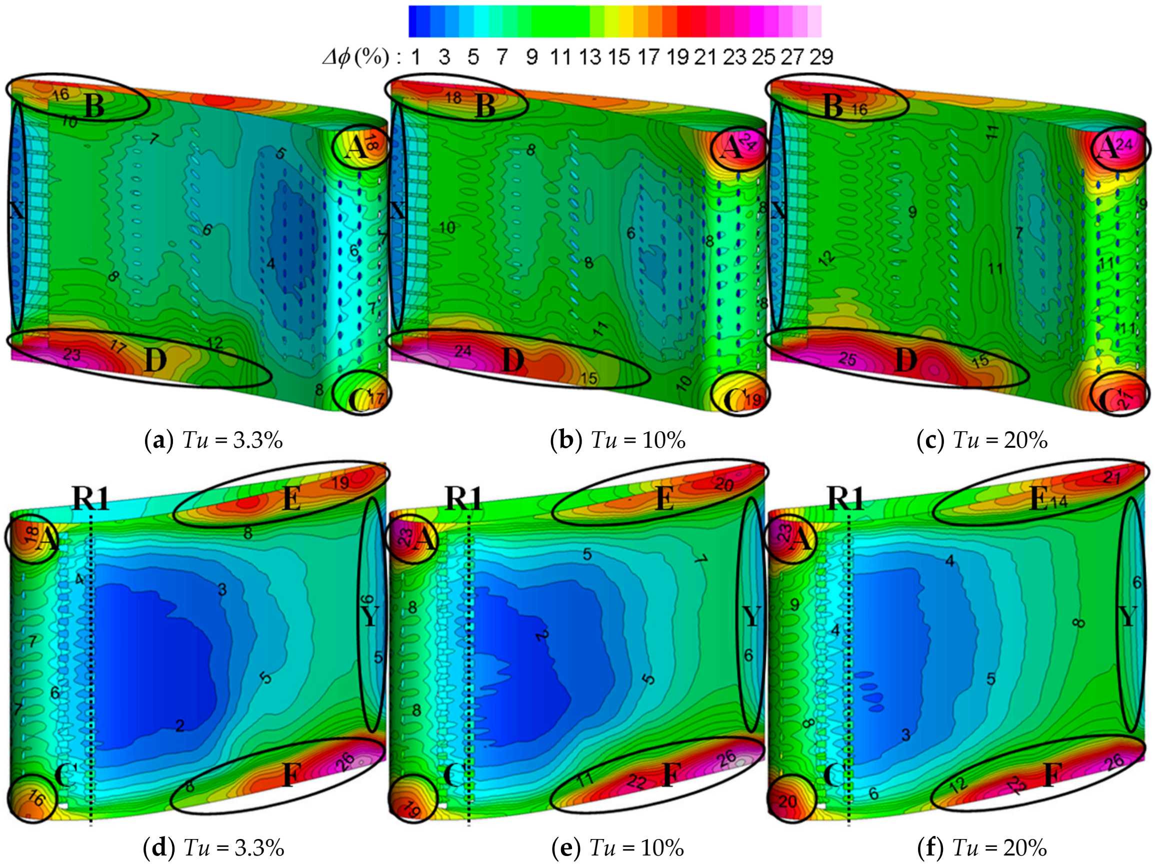

Figure 11. Effects of TBC on overall cooling effectiveness (**a**–**c**) on the PS; (**d**–**f**) on the SS at three *Tus*.

5.3. Effects of TBC and Tu on Heat Transfer Coefficient

Figure 12 shows the contours of Δh for the three *Tus*. It is shown that at each *Tu*, Δh is positive in the regions to be poorly cooled by cooling air, particularly between holes *R*12 and *R*13, *R*2 and *R*3, and the front of the TE on the SS as marked as regions 1, 2, and 3, respectively. This phenomenon suggests that TBC decreases the heat flux from the mainstream into the vane, and plays a positive role. However, the negative Δh is observed in the effectively cooled regions, especially at the exits of the film holes and the downstream regions of the shaped-hole *R*1. At this time TBC shows an opposite role and TBC blocks the heat flux from being released from the solid vane into the mixing fluid of cooling air with the mainstream. At the higher *Tus*, the roles of TBC on the heat transfer coefficient are more significant, as shown in Figure 13. The temperature distributions at midspan of the vane and mainstream are displayed at three *Tus* both with and without TBC. For each *Tu*, the effects of TBC on the mixing process of the mainstream and coolant is insignificant. However, the increase in *Tu* disturbs the cooling air near the exit and downstream of the film holes, and intensifies the mixing of the mainstream with cooling air. This causes higher temperatures in the vane and higher heat transfer. Therefore, the role of TBC increases, and this phenomenon is evident on the PS. The enhanced mixing of the mainstream with cooling air is more clearly shown in Figure 14.

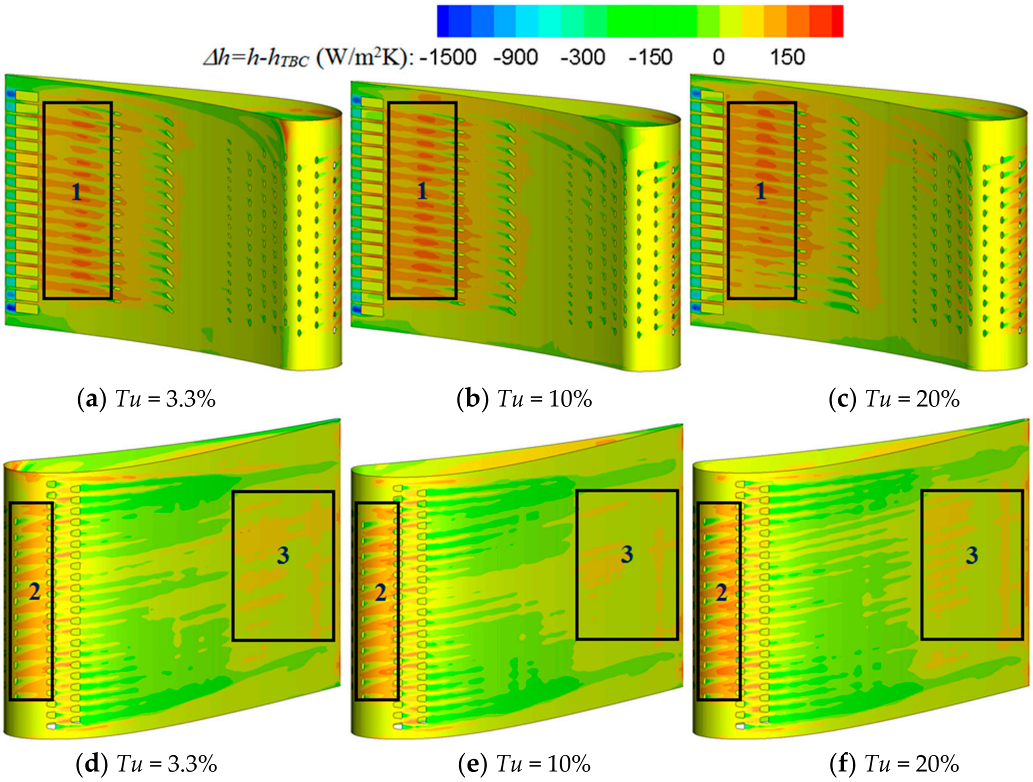

Figure 12. Effect of TBC on heat transfer coefficient (**a**–**c**) on the PS; (**d**–**f**) on the SS at three *Tus*.

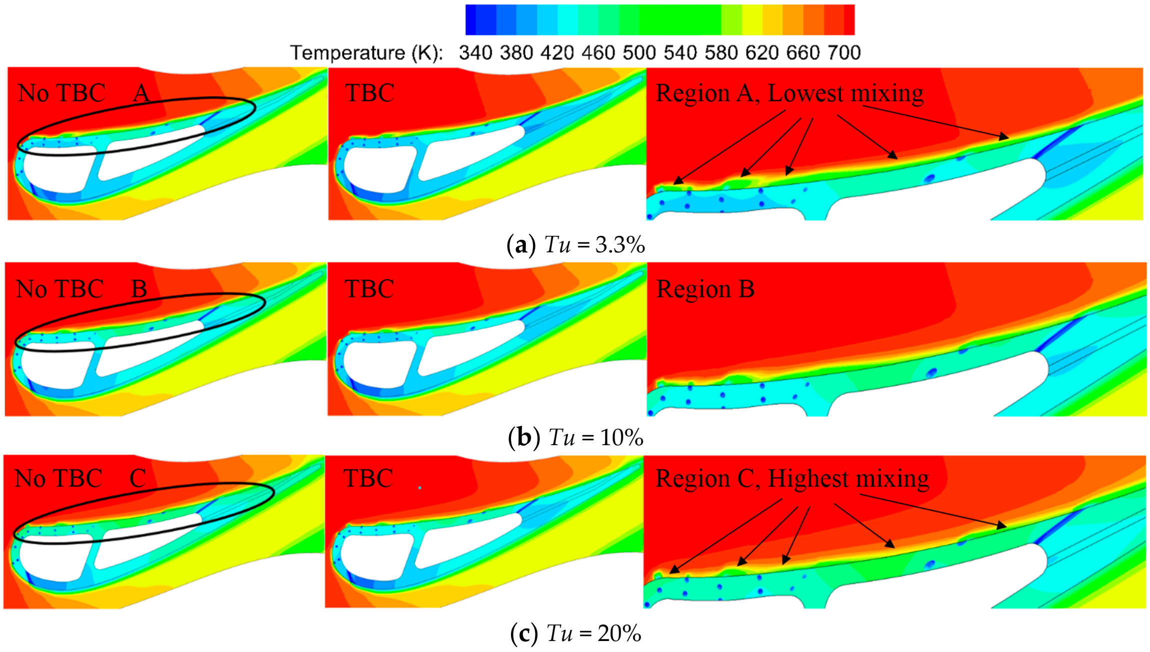

Figure 13. Effect of *Tu* on cooling air emitted from film holes at midspan.

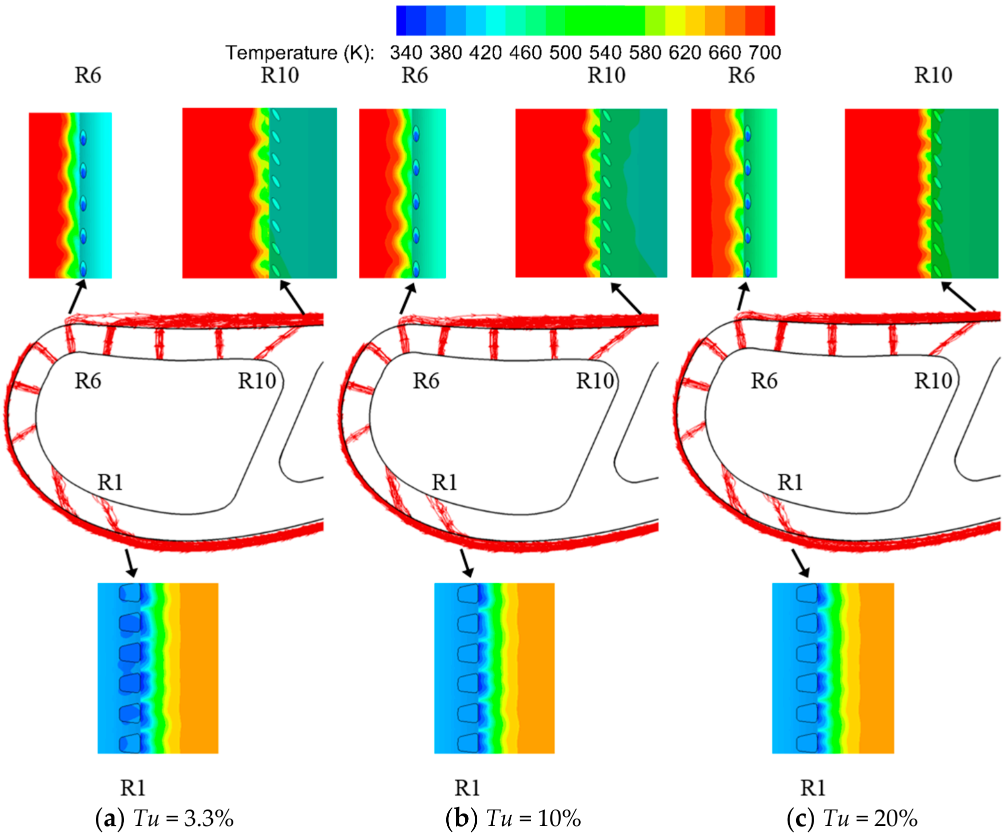

Figure 14. Effect of *Tu* on streamtraces of cooling air emitted from the film holes at midspan.

Figure 14 demonstrates, for the vane without TBC at the three *Tus*, streamtraces of the cooling air released from the inlets of the film holes at midspan and contours of temperature in the plane perpendicular to the axial chord and immediately downstream of film-hole rows *R*1, *R*6 and *R*10. As *Tu* increases from 3.3% to 20%, the streamtraces coming out of film-hole rows *R*6 and *R*10 are disturbed more strongly than those of film-hole rows *R*1. Furthermore, the enhanced mixing at higher *Tus* of the mainstream and cooling air can be evidenced from the contours of temperature. These phenomena show that the higher mainstream *Tus* cause higher disturbances to the cooling air emitted on the PS than on the SS.

6. Conclusions

This paper presents a numerical investigation on the combined effects of TBC and *Tu* on the cooling performances of a modified vane of the film-cooled nozzle guide vane (NGV). The overall cooling effectiveness, TBC effectiveness and heat transfer coefficient are analyzed and discussed at *Tu* = 3.3%, 10% and 20%. Through the comparisons and discussions, the following conclusions are drawn. However, it should be noted that because of the lack of experimental data for heat transfer in the report of Timko [26], a heat transfer comparison with the experimental data is not drawn. Therefore, the conclusions drawn here should be extended cautiously.

(1) TBC increases significantly the overall cooling effectiveness on the basis of the vane metal surface, but it does not alter the trends of distribution of the overall cooling effectiveness for all three Tus.

(2) For this test case, with only two rows of film holes on the SS, TBC is more effective on the PS than on the SS. The role of TBC on the increment in the overall cooling effectiveness is relatively higher in the ineffectively cooled regions, i.e., the tip and hub of the vane, but is relatively lower in the regions close to the exits of film holes, the downstream of the diffusion shaped-holes on the SS, and the TE.

(3) When Tu increases, the increment in the overall cooling effectiveness due to TBC in the ineffectively cooled regions can reach up to 24% or 38 K at Tu = 20%, but increases slightly in the exits and downstream of the diffusion shaped-holes on the SS, as well as the TE.

(4) TBC can block heat flux from mainstream into the vane, but it can also blocks the heat flux transferred from the solid vane into the mixing fluid of cooling air and the mainstream. When Tu increases, these effects becomes more significant.

Acknowledgments: The research is supported by the Natural Science Foundation of China (Contract No. 51376168). The first author gratefully acknowledges the support of the Chinese Academy of Sciences (CAS) and the World Academy of Sciences (TWAS) for providing the opportunity to study and research at the University of Science and Technology of China with the CAS-TWAS President's Fellowship Programme for the Ph.D. Candidates from Developing Countries.

Author Contributions: In this paper, Prasert Prapamonthon designed the methodology, carried out the calculation, analyzed the numerical results, and wrote this paper; Huazhao Xu proposed the idea of applying FLUENT to simulate the effect of thermal barrier coating, and improved the discussions; Wenshuo Yang improved the discussions; and Jianhua Wang improved this paper overall.

Conflicts of Interest: The authors declare no conflict of interest.

Nomenclature

$c_{p,f}$	specific heat capacity of fluid (J/kg·K)
$c_{p,m}$	specific heat capacity of solid (J/kg·K)
$c_{p,TBC}$	specific heat capacity of TBC (J/kg·K)
h	heat transfer coefficient at metal surface (W/m^2·K)
h_{TBC}	heat transfer coefficient at TBC surface (W/m^2·K)
Δh	variation of heat transfer coefficient (W/m^2·K)
k_f	thermal conductivity of fluid (W/m·K)
k_m	thermal conductivity of solid (W/m·K)
k_{TBC}	thermal conductivity of TBC (W/m·K)
Lu	turbulence length scale (m)
P	pressure (Pa)
PR	pressure ratio $[PR = \frac{P_T}{P_S}]$
P_s	static pressure (Pa)
$P_{T,c}$	total pressure at coolant inlet (Pa)
$P_{T,\infty}$	total pressure at mainstream inlet (Pa)
P_{ref}	reference pressure (3.44740×10^5 Pa)
q_{flux}	heat flux at the interface of solid and fluid (W/m^2)
R	percentage of metal temperature reduction (%)
T	metal surface temperature without TBC (K)
T_c	inlet temperature of cooling air (K)
T_{ref}	reference temperature (709 K)
T_{TBC}	metal surface temperature with TBC (K)
T_w	vane local wall temperature (K)
T_∞	inlet temperature of mainstream (K)
T'	TBC surface temperature (K)
Tu	free-stream turbulence intensity (%)
ΔT	temperature reduction in metal surface
$\left(\frac{\partial T}{\partial n}\right)_{w=0}$	temperature gradient at the interface of solid and fluid (K/m)
Greek Symbols	
ρ_f	density of mainstream and coolant (kg/m^3)
ρ_m	density of metal (kg/m^3)
ρ_{TBC}	density of TBC (kg/m^3)
ϕ	overall cooling effectiveness on the metal surface without TBC

ϕ_{TBC}	overall cooling effectiveness on the metal surface with TBC
τ	TBC effectiveness
$\Delta\phi$	increment of overall cooling effectiveness on the vane surface

References

1. Boyle, R.J.; Giel, P.W.; Ames, F.E. Predictions for the effects of free stream turbulence on turbine blade heat transfer. In Proceedings of the ASME Turbo Expo, Vienna, Austria, 14–17 June 2004.
2. Mayhew, J.E.; Baughn, J.W.; Byerley, A.R. The Effect of freestream turbulence on film cooling adiabatic effectiveness. *Int. J. Heat Fluid Flow* **2003**, *24*, 669–679. [CrossRef]
3. Ou, S.; Han, J.C. Influence of mainstream turbulence on leading edge film cooling heat transfer through two rows of inclined film slots. *J. Turbomach.* **1992**, *114*, 724–733. [CrossRef]
4. Ekkad, S.V.; Du, H.; Han, J.C. Local heat transfer coefficient and film effectiveness distributions on a cylindrical leading edge model using a transient liquid crystal image method. *J. Flow Vis. Image Process.* **1996**, *3*, 129–140. [CrossRef]
5. Thole, K.A.; Radomsky, R.W.; Kang, M.B.; Kohli, A. Elevated freestream turbulence effects on heat transfer for a gas turbine vane. *Int. J. Heat Fluid Flow* **2002**, *23*, 137–147. [CrossRef]
6. Dyson, T.E.; Bogard, D.G.; Bradshaw, S.D. A CFD evaluation of multiple RANS turbulence models for prediction of boundary layer flows on a turbine vane. In Proceedings of the ASME Turbo Expo, San Antonio, TX, USA, 3–7 June 2013.
7. Foroutan, H.; Yavuzkurt, S. A model for simulation of turbulent flow with high free stream turbulence implemented in OpenFOAM®. *J. Turbomach.* **2013**, *135*, 031022. [CrossRef]
8. Morata, E.C.; Gourdain, N.; Duchaine, F.; Gicquel, L.Y.M. Effects of free-stream turbulence on high pressure turbine blade heat transfer predicted by structured and unstructured LES. *Int. J. Heat Mass Trans.* **2012**, *55*, 5754–5768. [CrossRef]
9. Henze, M.; Bogdanic, L.; Muehlbauer, K.; Schnieder, M. Effect of the Biot number on metal temperature of thermal-barrier-coated turbine parts: Real engine measurements. *J. Turbomach.* **2013**, *135*, 031029. [CrossRef]
10. Witz, G.; Bossmann, H.-P. Determination of thermal barrier coatings average surface temperature after engine operation for lifetime validation. *J. Eng. Gas Turbines Power* **2012**, *134*, 122507. [CrossRef]
11. Davidson, E.T.; Kistenmacher, D.A.; Bogard, D.G. Film cooling with a thermal barrier coating: Round holes, craters and trenches. *J. Turbomach.* **2013**, *136*, 041007. [CrossRef]
12. Davidson, E.T.; Dees, J.E.; Bogard, D.G. An experimental study of thermal barrier coatings and film cooling on an internally cooled simulated turbine vane. In Proceedings of the ASME Turbo Expo, Vancouver, BC, Canada, 6–10 June 2011.
13. Meitner, P.L. *Analysis of Metal Temperature and Coolant Flow with a Thermal-Barrier Coating on a Full-Coverage Film Cooled Turbine Vane*; NASA Technical Report 78-20; NASA: Greenbelt, MD, USA, 1978.
14. Feuerstein, A.; Knapp, J.; Taylor, T.; Ashary, A.; Bolcavage, A.; Hitchman, N. Technical and economical aspects of current thermal barrier coating systems for gas turbine engines by thermal spray and EBPVD: A review. *J. Therm. Spray Technol.* **2008**, *17*, 199–213. [CrossRef]
15. Ni, R.H.; Humber, W.; Fan, G.; Johnson, P.D.; Downs, J.; Clark, J.P.; Koch, J.P. Conjugate heat transfer analysis of a film-cooled turbine vane. In Proceedings of the ASME Turbo Expo, Vancouver, BC, Canada, 6–10 June 2011.
16. Mazur, Z.; Herna'ndez-Rossette, A.; Garcı'a-Illescas, R.; Luna-Ramı'rez, A. Analysis of conjugate heat transfer of a gas turbine first stage nozzle. *Appl. Therm. Eng.* **2006**, *26*, 1796–1806. [CrossRef]
17. Yoshiara, T.; Sasaki, D.; Nakahashi, K. Conjugate heat transfer simulation of cooled turbine blades using unstructured-mesh CFD solver. In Proceedings of the AIAA 49th Aerospace Sciences Meeting including the New Horizons Forum and Aerospace Exposition, Orlando, FL, USA, 4–7 January 2011.
18. Zhang, H.J.; Zou, Z.P.; Li, Y.; Ye, J.; Song, S.H. Conjugate heat transfer investigations of turbine vane based on transition models. *Chin. J. Aeronaut.* **2013**, *26*, 890–897. [CrossRef]

19. Hylton, L.D.; Mihelc, M.S.; Turner, E.R.; Nealy, D.A.; York, R.E. *Analytical and Experimental Evaluation of the Heat Transfer Distribution over the Surface of Turbine Vanes*; NASA No. CR-168015; NASA: Greenbelt, MD, USA, 1983.
20. Bohn, D.E.; Becker, V.J. A conjugate 3-D flow and heat transfer analysis of a thermal barrier cooled turbine guide vane. In Proceedings of the ASME the International Gas Turbine & Aeroengine Congress & Exhibition, Stockholm, Sweden, 2–5 June 1998.
21. Baldwin, B.S.; Lomax, H. Thin layer approximation and algebraic model for separated turbulent flows. In Proceedings of the AIAA 16th Aerospace Sciences Meeting, Huntsville, AL, USA, 6–18 January 1978.
22. Bohn, D.E.; Tümmers, C. Numerical 3-D conjugate flow and heat transfer investigation of a transonic convection-cooled thermal barrier coated turbine guide vane with reduced cooling fluid mass flow. In Proceedings of the ASME Turbo Expo, Atlanta, GA, USA, 16–19 June 2003.
23. Alizadeh, M.; Izadi, A.; Fathi, A. Sensitivity analysis on turbine blade temperature distribution using conjugate heat transfer simulation. *J. Turbomach.* **2014**, *136*, 011001. [CrossRef]
24. Rossette, A.H.; Mazur C, Z.; Demeulenaere, A.; Roque López Hernández, J.A. The effect of start-up cycle in ceramic coating used as thermal barrier for a gas turbine bucket. *Appl. Therm. Eng.* **2009**, *29*, 3056–3065. [CrossRef]
25. Spalart, P.R.; Allmaras, S.R. A one equation turbulence model for aerodynamic flows. In Proceedings of the 30th Aerospace Sciences Meeting & Exhibit, Reno, NV, USA, 6–9 January 1992.
26. Timko, L.P. *Energy Efficient Engine High Pressure Turbine Component Test Performance Report*; NASA CR-168289; NASA Lewis Research Center: Cleveland, OH, USA, 1984.
27. Halila, E.E.; Lenahan, D.T.; Thomas, T.T. *High Pressure Turbine Test Hardware Detailed Design Report*; NASA CR-167955; NASA Lewis Research Center: Cleveland, OH, USA, 1982.
28. Zhang, Q.B.; Xu, H.Z.; Wang, J.H.; Li, G.; Wang, L.; Wu, X.Y.; Ma, S.Y. Evaluation of CFD predictions using different turbulence models on a film cooled guide vane under experimental conditions. In Proceedings of the ASME Turbo Expo, Montreal, QC, Canada, 15–19 June 2015.
29. Prapamonthon, P.; Xu, H.Z.; Wang, J.H.; Li, G. Predicting adiabatic film effectiveness of a turbine vane by two-equation turbulence models. In Proceedings of the ASME Turbo Expo, Montreal, QC, Canada, 15–19 June 2015.
30. Ke, Z.Q.; Wang, J.H. Numerical investigations of pulsed film cooling on an entire turbine vane. *Appl. Therm. Eng.* **2015**, *87*, 117–126. [CrossRef]
31. Kingery, J.E.; Ames, F.E. Full coverage shaped-hole film cooling in an accelerating boundary layer with high freestream turbulence. *J. Turbomach.* **2016**, *138*, 071002. [CrossRef]